


Cite this: *RSC Adv.*, 2017, 7, 25347Received 23rd February 2017
Accepted 5th May 2017

DOI: 10.1039/c7ra02274c

rsc.li/rsc-advances

Modelling of an equivalent circuit for $\text{Cu}_2\text{ZnSnS}_4$ - and $\text{Cu}_2\text{ZnSnSe}_4$ -based thin film solar cells†

Naoyuki Shibayama,^a *^a Yiwen Zhang,^a Tetsuo Satake^a and Mutsumi Sugiyama^b

The internal resistance and quality of the interface in $\text{Cu}_2\text{ZnSn(S, Se)}_4$ (CZT(S, Se)) solar cells were investigated using electrochemical impedance spectroscopy (EIS). We developed an equivalent circuit of the CZT(S, Se) solar cell involving the contact and material resistances R_{bulk} , two parallel resistances, and a 'capacitance-like element' called a constant phase element (CPE) around the CZT(S, Se)/CdS heterojunction and Mo–Mo(S, Se)₂/CZT(S, Se) back-contact interfaces. Using the EIS method, the states of Mo(S, Se) and the CZT(S, Se) layer could be digitised non-destructively. This result can provide guidelines for improving the performance of CZT(S, Se) solar cells or any semiconductor device.

Introduction

$\text{Cu}_2\text{ZnSn(S, Se)}_4$ (CZT(S, Se)) materials have been extensively studied for use in next-generation solar cells because they can be produced with inexpensive materials and processes.¹ The energy conversion efficiency of CZT(S, Se) solar cells has reached 12.6%;² however, this is remarkably lower than that of cadmium telluride (CdTe, 22.1%) and copper indium gallium selenide (CIGS, 22.6%) based solar cells.³

Many studies have been carried out to identify the major hurdles that influence the CZT(S, Se) solar cell performance, such as composition defects, interface energy band gap, and structure. In addition, the elimination or passivation of Cu–Zn disorder can be very important for improving the efficiency of CZT(S, Se) solar cells.⁴

It is widely accepted that charge recombination at the interface is one possible cause of V_{oc} degradation.⁵ Therefore, understanding charge transfer and charge recombination at different interfaces is important for improving the performance of CZTS solar cells. It is reported that CZTS/CdS interface has shown a cliff configuration which contributes to carrier losses.⁶ On the other hand, the interface of Mo/Mo(S, Se)/CZT(S, Se) are the stage at which research is currently underway.

One strategy to enhance the performance of CZT(S, Se) solar cells are (1) to control the chemical composition of the CZT(S, Se) absorber layer to improve efficiency⁷ and (2) to modify the back contact/absorber⁸ and absorber/buffer⁹ layer interfaces. However, clear guidelines for the correlation between the device

performance and internal issues such as the absorber layer and interface of the devices have not yet been established.

Electrochemical impedance spectroscopy (EIS) is a non-destructive technique for examining electrochemical devices using transfer functions¹⁰ such as the impedance of the equivalent circuits of CdTe,¹¹ CIGS,¹² dye-sensitised,¹³ and perovskite solar cells.¹⁴ The advantage of EIS is to provide comprehensive data to evaluate both the capacitance of the complex stacked layers and the quality and uniformity of the interfaces. In our previous studies, the EIS method was applied to investigate CIGS solar cells,^{12b–d} and the state of the pn junction interface was confirmed, which are issues that are difficult to investigate using other techniques such as capacitance measurements, admittance spectroscopy, and deep-level transient spectroscopy.

In this study, we used EIS to investigate the internal situation of CZT(S, Se) solar cells and improve their photovoltaic performance. An experimental model was developed to compare the Mo(S, Se)₂ thickness of CZT(S, Se) solar cells and examine defects in the CZT(S, Se) absorber layer. This study demonstrated that EIS can be used to characterise the CZT(S, Se)/CdS heterojunction and non-ohmic Mo–Mo(S, Se)₂/CZT(S, Se) back-contact interfaces. Our findings can provide guidance to improving the performance of CZT(S, Se) solar cells.

Results and discussion

In general, an equivalent circuit of simple heterojunction materials consists of three elements: the contact and material resistances R_{bulk} , parallel circuit with the parallel resistance R_{p} , and constant capacitance C or capacitance-like element called a constant phase element (CPE). A CPE displays impedance with non-ideal frequency-dependent properties and a constant phase over the entire frequency. The non-ideal behaviour originates from the distribution of the current density due to material

^aTechnical Research Institute, Toppan Printing Co., Ltd., Sugito, 345-8508, Japan.
E-mail: naoyuki.shibayama@toppan.co.jp

^bDepartment of Electrical Engineering, Faculty of Science and Technology, Tokyo University of Science, Noda 278-8510, Japan

† Electronic supplementary information (ESI) available. See DOI: 10.1039/c7ra02274c



inhomogeneity.^{12b,c} The impedance of a CPE (Z_{CPE}) is defined by the CPE index p (CPE- p) and CPE constant T (CPE- T) as follows:

$$Z_{CPE} = \frac{1}{(j\omega)^p T} \quad (1)$$

Fig. 1 shows Nyquist plots for each of the equivalent circuits. The horizontal axis (real axis) represents the resistance, and the normal axis (imaginary axis) represents the capacitance of the equivalent circuit. For the equivalent circuit using C , the diameter of the semicircle represents R_p , and the value of the intersection to the right of the semicircle and the horizontal axis represents R_{bulk} , as shown in Fig. 1(a). The Nyquist plot of the equivalent circuit using a CPE makes single semicircles with their centres lying below the imaginary axis, as shown in Fig. 1(b). Here, j is a complex number, and ω is the angular frequency. The value of CPE- p (where $0 \leq p \leq 1$) reflects the uniformity and quality of the interface. As the value of CPE- p approaches 1, a higher-quality uniformity and interface can be ascertained by observing the cross section.

As summarised in Table 1 and Fig. 2, conversion efficiencies of 4.25% and 0.75% were obtained for the CZTS and CZTSe solar cells, respectively. As shown in Fig. 3, the edge of external quantum efficiency (EQE) spectra of the CZTS and CZTSe solar cells were about 950 nm and 1280 nm, respectively. The EQE values obtained for CZTSe solar cell in the whole region is markedly remarkably lower than that for CZTS solar cell. Fig. 4 shows the X-ray diffraction (XRD) patterns of the Mo/MoSe₂/CZTS and Mo/MoSe₂/CZTSe layers, respectively. In the Mo/MoSe₂/CZTS layer, CZTS crystal and Mo which are the substrate constituents were observed. On the other hand, in Mo/MoSe₂/CZTSe layer, in addition to CZTSe and Mo, patterns derived from MoSe₂ were observed. As a result of XRD, it was confirmed that selenium (Se) was not contained in the CZTS layer and sulfur (S) was not contained in the CZTSe layer. It was confirmed that Mo reacts more easily with Se than S.¹⁵ In both

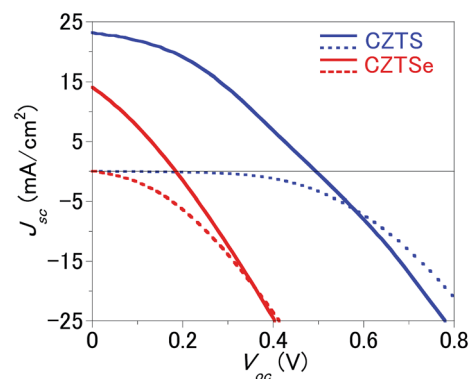


Fig. 2 J - V curves of CZTS and CZTSe solar cells.

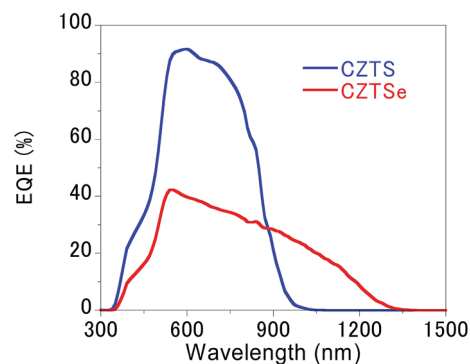


Fig. 3 Measured EQE spectra of CZTS and CZTSe solar cells employed in this work.

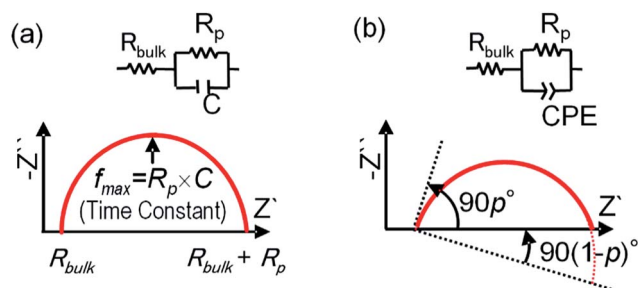


Fig. 1 Equivalent circuits and Nyquist plots of simple heterojunction materials consisting of three elements: R_{bulk} , R_p , and (a) C or (b) CPE .

Table 1 Solar cell performances of CZTS and CZTSe solar cells

Cell	Efficiency (%)	FF (—)	V_{oc} (V)	J_{sc} (mA cm ⁻²)
CZTS	4.25	0.494	0.371	23.17
CZTSe	0.75	0.290	0.184	14.04

photoharvesting layers of CZTS and CZTSe, respective constituent elements copper (Cu), zinc (Zn), tin (Sn), sulfur (S) and selenium (Se) distribution is uniform and exist homogeneously. The distribution of each element in the film is shown in our previously published report.¹⁶

A cross-sectional Scanning Ion Microscope (SIM) with a slope of 60 degrees is shown in Fig. 5. The thickness of the absorption layers in CZTS and CZTSe are measured to be around 1.3 μ m and 1.5 μ m for the CZT(S, Se) layer respectively. In our previous study, a possible interpretation for this much poorer performance of the CZTSe solar cell is that Cu-rich regions in the CZTSe layer provide a leakage current path.¹⁶ The thickness of the Mo(S, Se)₂ layer compared with that of the CZTS solar cell may be another reason for the low efficiency of the CZTSe solar cell.^{8d} To obtain further insight into the performances of CZTS and CZTSe solar cells, EIS was used to measure the resistance and quality of the thick CZT(S, Se)/CdS heterojunction and non-ohmic Mo-Mo(S, Se)₂/CZT(S, Se) back contact interfaces of CZTS and CZTSe solar cells.

Fig. 6 shows the four equivalent circuit models tested to adjust the impedance data: M1-M4. The simplest model (M1) corresponded to a device characterised by the contact and material resistances R_{bulk} and two consecutive circuit elements consisting of a capacitor and resistor in parallel (C_1 - R_1 , C_2 - R_2). The first element modelled all of the contact and material resistances R_{bulk} , such as the Mo contact, ZnO:Al front window,



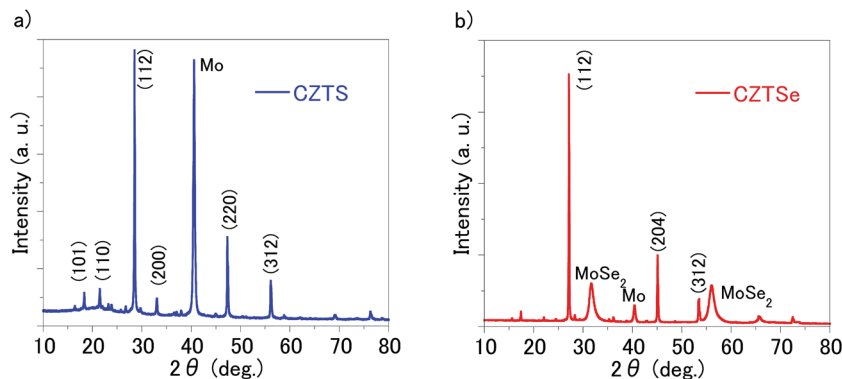


Fig. 4 XRD patterns of (a) Mo/MoSe₂/CZTS and (b) Mo/MoSe₂/CZTSe layers.

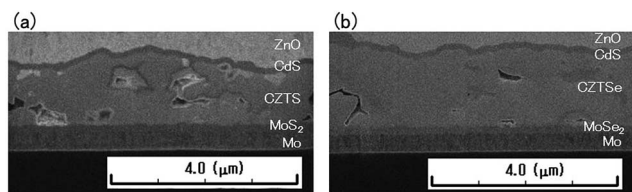


Fig. 5 SIM image of cross-sectional surface of (a) CZTS_{cell} and (b) CZTSe_{cell}.

and Ag:Mo contact grid. The capacitors and resistors in parallel corresponding to the low- and high-frequency sides of the Nyquist plots described the CZT(S, Se)/CdS heterojunction (Fig. 6, shaded by the blue box) and the non-ohmic Mo–Mo(S, Se)₂/CZT(S, Se) electrical back contact (Fig. 6, shaded by red box) in the AC response, respectively. Model M1 defined that the chemical composition and shape around the CZT(S, Se)/CdS and Mo–Mo(S, Se)₂/CZT(S, Se) interfaces are uniform. The

second model (M2) replaced C_1 – R_1 of M1 with CPE_1 – R_1 . M2 defined that the chemical composition and shape around the CZT(S, Se)/CdS heterojunction interface was non-uniform. The third model (M3) replaced C_2 – R_2 of M1 with CPE_1 – R_1 . M3 defined that the chemical composition and shape around the Mo–Mo(S, Se)₂/CZT(S, Se) interface were non-uniform. The last model (M4) replaced C_1 – R_1 and C_2 – R_2 of M1 with CPE_1 – R_1 and CPE_2 – R_2 , respectively. M4 defined that the chemical composition and shape around the CZT(S, Se)/CdS and Mo–Mo(S, Se)₂/CZT(S, Se) interfaces were non-uniform.

Fig. 7 shows Bode plots of the impedances of the CZTS and CZTSe solar cells. There were two critical frequencies with magnitudes of around 10^3 to 10^4 and 10^5 to 10^6 Hz for the CZT(S, Se)/CdS and Mo–Mo(S, Se)₂/CZT(S, Se) interfaces, respectively. This result is consistent with the admittance spectroscopy result.¹⁷ The CZTS and CZTSe solar cells were confirmed to be composed of R_{bulk} and two parallel assemblies of C – R or CPE – R . In other words, they can be represented by any of the four equivalent circuit models in Fig. 6.

Fig. 8, S1 and S2† show the Nyquist plots and fitting results for the impedances of the CZTS and CZTSe solar cells. The chi-squared function (χ^2) provides a good indication of the quality adaptation; a lower value indicates a better match rate.¹⁸ As a result of the fitting, it was found that M4 is the most suitable equivalent circuit model. The Mo(S, Se)₂ layer has a graded structure in which the proportions of S and Se decrease and the proportion of Mo increases as the Mo layer is approached; further, Cu is added.¹⁶ Fig. 2 shows that the J – V curves of both CZT(S, Se) solar cells cause crossovers. Thus, the resistance near the interface of the Mo(S, Se)₂/CZT(S, Se) layer is high. In other words, the region close to the interface between the thick Mo(S, Se)₂ layer and CZT(S, Se) layer in particular has a heterogeneous composition. Consequently, because CPE_2 – R_2 was selected for Mo–Mo(S, Se)₂/CZT(S, Se), M3 and M4 are compatible equivalent circuit models. Because the CZTS layer at the CZT(S, Se)/CdS interface was coated by the spray method, the interface shape tended to become uneven. Moreover, a large number of point defects and boundaries are present. Therefore, CPE_1 – R_1 becomes the optimum combination of capacitances and resistances at the CZT(S, Se)/CdS interface. Thus, the equivalent circuit models M2 and M4 were selected. As a result of fitting

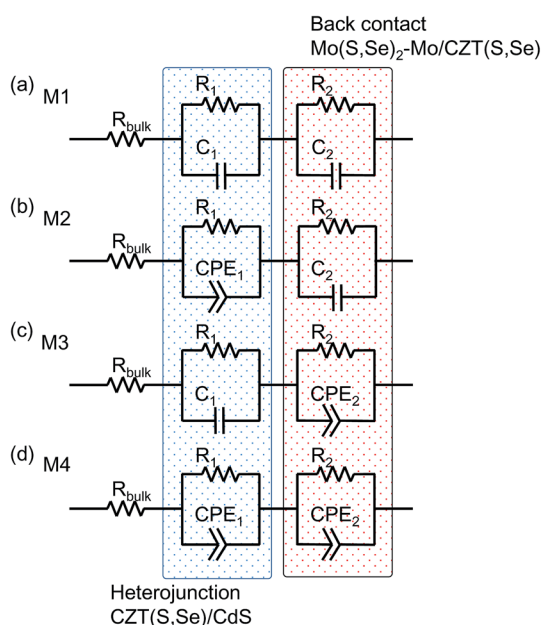


Fig. 6 Tested equivalent circuits of the CZTS and CZTSe solar cells.



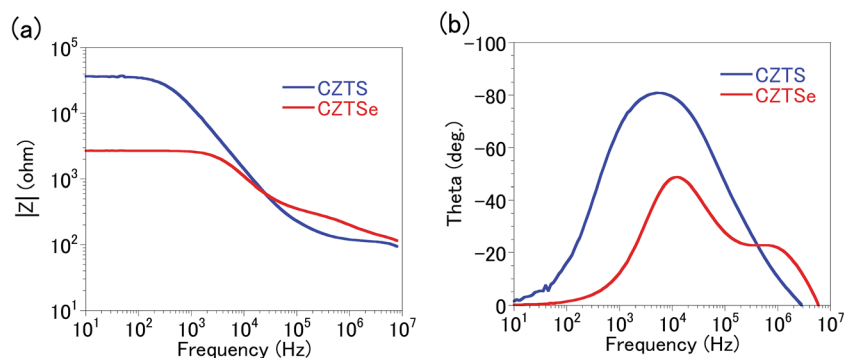


Fig. 7 Bode plots of CZTS and CZTSe solar cells: (a) amplitude $|Z|$ and (b) phase.

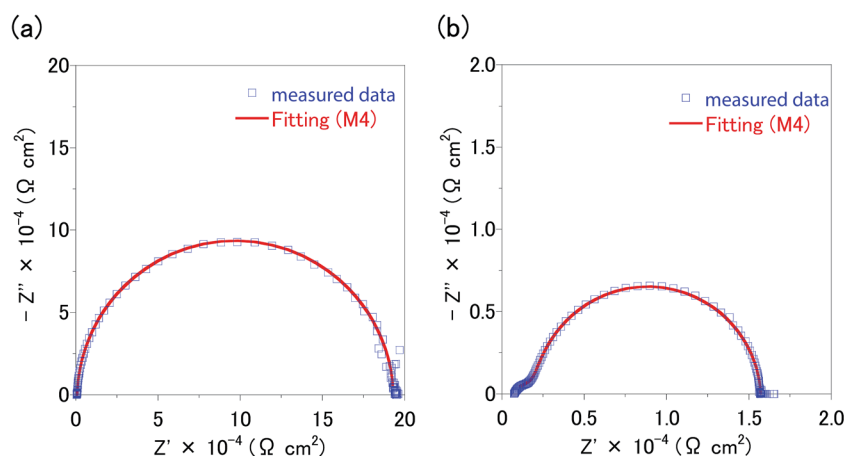


Fig. 8 Nyquist plots and fitting results of (a) CZTS and (b) CZTSe solar cells.

Table 2 Fitted parameters for electrochemical impedance spectra of CZTS and CZTSe solar cells

Cell	$R_{\text{bulk}} (\Omega \text{ cm}^2)$	$R_1 (\Omega \text{ cm}^2)$	$\text{CPE}_{1-p} (-)$	$R_2 (\Omega \text{ cm}^2)$	$\text{CPE}_{2-p} (-)$
CZTS	6.2×10^2	1.9×10^5	0.983	2.8×10^2	0.954
CZTSe	5.4×10^2	1.3×10^4	0.972	1.7×10^3	0.591

and interface, the M4 was selected as the equivalent circuit model of the CZTS and CZTSe solar cells.

EIS was performed under dark conditions to obtain further insight into the interface properties of the CZTS and CZTSe solar cells. Table 2 presents the corresponding EIS parameters. The value of the resistance R_2 around the Mo–Mo(S, Se)₂/CZT(S, Se) interface in the CZTS solar cell was $2.8 \times 10^2 \Omega \text{ cm}^2$, which is 5.5 times less the value of that obtained for the CZTSe solar cell ($1.7 \times 10^3 \Omega \text{ cm}^2$). Based on the results of the cross-sectional SIM images, the CZTSe solar cell had a thicker Mo(S, Se)₂ layer than the CZTS solar cells. This result is consistent with the EIS results. The CZTSe solar cell was observed to have a CPE_{1-p} value lower than that of the CZTS solar cell. This is because that thicker Mo(S, Se)₂ layer should lower the uniformity and quality of the Mo–Mo(S, Se)₂/CZT(S, Se) interface. The value of the resistance R_1 around the CZT(S, Se)/CdS interface in the CZTS solar cell was $1.9 \times 10^5 \Omega \text{ cm}^2$, and the value obtained for the

CZTSe solar cell ($1.3 \times 10^4 \Omega \text{ cm}^2$) was 7% of that CPE_{2-p} indicates the state of the CZT(S, Se)/CdS interface, and its values for the CZTS and CZTSe solar cells were nearly identical. A CdS layer was fabricated by the same procedure. The resistance R_1 was considered to be influenced by the CZT(S, Se) layer. Our previous results showed that Cu-rich regions of the CZT(S, Se) layer provide a leakage current path in the CZTSe cells.¹⁶ Therefore, the value of the resistance R_1 in the CZTSe solar cell was considered to be less than that expected from the leakage current paths.

Conclusions

We used EIS to develop an equivalent circuit model for CZT(S, Se) solar cells. By using the EIS method, it was demonstrated that the causes of the performance degradation of the CZT(S, Se) solar cells are the leakage current path in the CZT(S, Se)



layer, the resistance, and the lower uniformity and quality of the thicker Mo(S, Se)₂ layer. In other words, *via* analysis with the EIS method, it was possible to formulate guidelines for non-destructively improving the performance of CZT(S, Se) solar cells. We are able to suggest one of the guidelines for improving the conversion efficiency of CZT(S, Se) solar cells. Moreover the scope of this paper lies in devising a model for further understanding and advancement in the existing technology. This suggests that the abundance of experience and knowledge gained through the development of high-efficiency conventional solar cells can be applied to CZT(S, Se) solar cells.

Experimental section

Materials and measurement

CuI, ZnI₂, SnI₄, and Se were purchased from Sigma-Aldrich Co. LLC. S, and Na₂Se were purchased from Kojundo Chemical Lab. Co., Ltd. NaSe and thiourea were purchased from Kanto Chemical Co., Inc. All solvents and reagents were of the highest quality available and were used as received.

The photocurrent–voltage (*J*–*V*) characteristics of the CZTS and CZTSe solar cell were measured on a Keithley 2611A source meter under irradiation of AM 1.5, 100 mW cm^{−2} (1 sun) supplied by a solar simulator (Otento-SunIII, Bunkoukeiki Co., Ltd.). The incident light intensity was calibrated with a reference Si solar cell (SRC-1000-RTD-XL-J, VLSI Standards. Incorporated). The active areas of the solar cells were determined with a KEYENCE VHX-1000 digital microscope.

The impedance was measured with an NF FRA5087 frequency response analyser at frequencies of 100 mHz to 1 MHz. For all measurements, an AC 100 mV signal was applied to the device without a DC bias under dark conditions at room temperature. The obtained data were fitted with the Z-plot software.

Preparation of CZTS and CZTSe solar cells

CZT(S, Se) solar cells were fabricated following the same experimental conditions and protocol in the previously published literature.¹⁶

CuI (2.88 mmol), ZnI₂ (1.76 mmol), and SnI₄ (1.60 mmol) were added to pyridine (500 mL) as a metal source and then cooled to 0 °C by stirring until a clear solution was obtained. Na₂Se (6.4 mmol), a chalcogenide source, was dissolved in methanol (125 mL) and then quickly transferred into the metal source to synthesize CZTSe nanoparticles, as shown in the following reaction: 1.8CuI + 1.1ZnI₂ + SnI₄ + 4Na₂Se → Cu_{1.8}Zn_{1.1}Sn_{1.0}Se₄ + 8NaI. The reaction was carried out under N₂ atmosphere at 0 °C for 30 min. The products were centrifuged and washed three times with solvent (pyridine–methanol = 4 : 1) to remove the byproduct of NaI. The products were dispersed into pyridine/methanol solvents by sonication for 20 min. The cation ratios of the CZTSe nanoparticles (denoted as CZTSe nanoparticles) measured by EDS were Cu/(Zn + Sn) = 0.80 and Zn/Sn = 1.11. Thiourea was added into the as-synthesized CZTSe nanoparticles as a binder followed by spraying onto Mo-coated substrates heated at 250 °C using an

ultrasonic spray system (Sono-Tek Exacta Coat). Then, sintering treatments were carried out under sulfur or selenium atmospheres. For sintering, the samples were placed in a quartz box of 16 cm³ volume and then sintered at 580 °C for 20 min under N₂ atmosphere at atmospheric pressure. To prevent the loss of Sn and S during the sintering process, 10 mg of Sn powder and 48 mg of S powder were added in the box. For selenium sintering, the process was the same as that of sulfur sintering except that 10 mg of Sn and 40 mg of Se were used.

Finally, solar cells with a structure of Al grid/B-doped ZnO/i-ZnO/CdS/CZT(S, Se)/Mo/soda-lime glass were fabricated. Here, CdS buffer layers were deposited by chemical bath deposition (CBD). Intrinsic ZnO and B-doped ZnO layers were deposited by metal organic chemical vapor deposition (MOCVD). Al grid electrodes were deposited by vacuum evaporation. The structure of the fabricated CZT(S, Se) solar cells are Mo/Mo(S, Se)₂/CZT(S, Se)/CdS/ZnO/Al respectively. The area of the solar cell measured for photovoltaic performance was about 0.125 cm².

Acknowledgements

The authors thank N. Suyama, and Professor A. Yamada for discussions. This research was partially supported by the Japan Science and Technology Agency, Advanced Low Carbon Technology Research and Development Program.

References

- (a) S. Ito, *Wiley Interdiscip. Rev.: Energy Environ.*, 2015, **4**, 51; (b) H. Zhou, W.-C. Hsu, H.-S. Duan, B. Bob, W. Yang, T.-B. Song, C.-J. Hsu and Y. Yang, *Energy Environ. Sci.*, 2013, **6**, 2822; (c) K. Kaur, N. Kumara and M. Kumar, *J. Mater. Chem. A*, 2017, **5**, 3069.
- W. Wang, M. T. Winkler, O. Gunawan, T. Gokmen, T. K. Todorov, Y. Zhu and D. B. Mitzi, *Adv. Energy Mater.*, 2014, **4**, 1301465.
- M. A. Green, K. Emery, Y. Hishikawa, W. Warta, E. D. Dunlop, D. H. Levi and A. W. Y. Ho-Baillie, *Prog. Photovoltaics*, 2017, **1**, 3.
- (a) S. Susan, *Sol. Energ. Mat. Sol. Cells*, 2011, **95**, 1482; (b) A. Walsh, S. Chen, S.-H. Wei and X.-G. Gong, *Adv. Energy Mater.*, 2012, **2**, 400.
- O. Gunawana, T. K. Todorov and D. B. Mitzi, *Appl. Phys. Lett.*, 2010, **97**, 233506.
- (a) S. Siebentritt, *Thin Solid Films*, 2013, **535**, 1; (b) A. Polizzotti, I. L. Repins, R. Noufi, S.-H. Wei and D. B. Mitzi, *Energy Environ. Sci.*, 2013, **6**, 3171; (c) C. Yan, F. Liu, N. Song, B. K. Ng, J. A. Stride, A. Tadich and X. Hao, *Appl. Phys. Lett.*, 2014, **104**, 173901; (d) M. Courel, J. A. Andrade-Arvizu and O. Vigil-Galán, *Appl. Phys. Lett.*, 2014, **105**, 233501.
- (a) T. Toyama, T. Konishi, Y. Seo, R. Tsuji, K. Terai, Y. Nakashima, H. Okamoto and Y. Tsutsumi, *Appl. Phys. Express*, 2013, **6**, 075503; (b) D.-H. Son, D.-H. Kim, S.-N. Park, K.-J. Yang, D. Nam, H. Cheong and J.-K. Kang, *Chem. Mater.*, 2015, **27**, 5180; (c) W.-C. Chen, C.-Y. Chen, V. Tunuguntla, S. H. Lu, C. Su, C.-H. Lee, K.-H. Chen and



- L.-C. Chen, *Nano Energy*, 2016, **30**, 762; (d) Y. Qu, G. Zoppi and N. S. Beattie, *Sol. Energ. Mat. Sol. Cells*, 2016, **158**, 130; (e) J. Tao, K. Zhang, C. Zhang, L. Chen, H. Cao, J. Liu, J. Jiang, L. Sun, P. Yang and J. Chu, *Chem. Commun.*, 2015, **51**, 10337; (f) J. Tao, J. Liu, L. Chen, H. Cao, X. Meng, Y. Zhang, C. Zhang, L. Sun, P. Yang and J. Chu, *Green Chem.*, 2016, **18**, 550.
- 8 (a) B. Shin, Y. Zhu, N. A. Bojarczuk, S. Jay Chey and S. Guha, *Appl. Phys. Lett.*, 2012, **101**, 053903; (b) A. Fairbrother, E. Garcia-Hemme, V. Izquierdo-Roca, X. Fontane, F. A. Pulgarin-Agudelo, O. Vigil-Galan, A. Perez-Rodriguez and E. Saucedo, *J. Am. Chem. Soc.*, 2012, **34**, 8018; (c) S. Lopez-Marino, M. Espindola-Rodriguez, Y. Sánchez, X. Alcobé, F. Oliva, H. Xie, M. Neuschitzer, S. Giraldo, M. Placidi, R. Caballero, V. Izquierdo-Roca, A. Pérez-Rodríguez and E. Saucedo, *Nano Energy*, 2016, **26**, 708; (d) J. Li, Y. Zhang, W. Zhao, D. Nam, H. Cheong, L. Wu, Z. Zhou and Y. Sun, *Adv. Energy Mater.*, 2015, **5**, 1402178.
- 9 (a) H. Katagiri, K. Jimbo, S. Yamada, T. Kamimura, W. S. Maw, T. Fukano, T. Ito and T. Motohiro, *Appl. Phys. Express*, 2008, **1**, 041201; (b) S. Tajima, M. Umehara and T. Mise, *Jpn. J. Appl. Phys.*, 2016, **55**, 112302; (c) F. Jiang, C. Ozaki, Gunawan, T. Harada, Z. Tang, T. Minemoto, Y. Nose and S. Ikeda, *Chem. Mater.*, 2016, **28**, 3283; (d) F. Liu, C. Yan, J. Huang, K. Sun, F. Zhou, J. A. Stride, M. A. Green and X. Hao, *Adv. Energy Mater.*, 2016, **6**, 1600706; (e) Y. Ren, J. J. S. Scragg, M. Edoff, J. K. Larsen and C. Platzer-Björkman, *ACS Appl. Mater. Interfaces*, 2016, **8**, 18600.
- 10 (a) J. Bisquert, *Phys. Chem. Chem. Phys.*, 2011, **13**, 4679; (b) I. Mora-Seró, G. Garcia-Belmonte, P. P. Boix, M. A. Vázquez and J. Bisquert, *Energy Environ. Sci.*, 2009, **2**, 678.
- 11 B. H. Hamadani, J. Roller, P. Kounavis, N. B. Zhitenev and D. J. Gundlach, *Sol. Energ. Mat. Sol. Cells*, 2013, **116**, 126.
- 12 (a) W.-J. Lee, H.-J. Yu, J.-H. Wi, D.-H. Cho, W. S. Han, J. Yoo, Y. Yi, J.-H. Song and Y.-D. Chung, *ACS Appl. Mater. Interfaces*, 2016, **8**, 22151; (b) M. Sugiyama, M. Hayashi, C. Yamazaki, N. B. Hamidon, Y. Hirose and M. Itagaki, *Thin Solid Films*, 2013, **535**, 287; (c) M. Sugiyama, H. Sakakura, S. W. Chang and M. Itagaki, *Electrochim. Acta*, 2014, **131**, 236; (d) H. Sakakura, M. Itagaki and M. Sugiyama, *Jpn. J. Appl. Phys.*, 2016, **55**, 012301.
- 13 (a) N. Shibayama, H. Ozawa, Y. Ooyama and H. Arakawa, *Bull. Chem. Soc. Jpn.*, 2015, **88**, 366; (b) N. Shibayama, H. Ozawa, M. Abe, Y. Ooyama and H. Arakawa, *Chem. Commun.*, 2014, **50**, 6398; (c) Y. Adachi, Y. Ooyama, N. Shibayama and J. Ohshita, *Dalton Trans.*, 2016, **45**, 13817.
- 14 (a) K. Miyano, M. Yanagida, N. Tripathi and Y. Shirai, *Appl. Phys. Lett.*, 2016, **106**, 093903; (b) I. Zarazua, G. Han, P. P. Boi, S. Mhaisalkar, F. Fabregat-Santiago, I. Mora-Seró, J. Bisquert and G. Garcia-Belmonte, *J. Phys. Chem. Lett.*, 2016, **7**, 5105.
- 15 M. Ganchev, *Thin Solid Films*, 2011, **519**, 7394.
- 16 Y. Zhang, N. Suyama, M. Goto, J. Kuwana, K. Sugimoto, T. Satake, Y. Kurokawa, M. Yin and A. Yamada, *Jpn. J. Appl. Phys.*, 2015, **54**, 08KC05.
- 17 (a) P. A. Fernandes, A. F. Sartori, P. M. P. Salome, J. Malaquias, A. F. da Cunha, M. P. F. Grac and J. C. Gonzalez, *Appl. Phys. Lett.*, 2012, **100**, 233504; (b) P. A. Fernandes, P. M. P. Salome, A. F. Sartori, J. Malaquias, A. F. Cunha, B. A. Schubert, J. C. Gonzalez and G. M. Ribeiro, *Sol. Energ. Mat. Sol. Cells*, 2013, **115**, 157.
- 18 M. Umeda, K. Dokko, Y. Fujita, M. Mohamedi, M. Umeda, I. Uchida and J. R. Selman, *Electrochim. Acta*, 2001, **47**, 885.

